Trichlorosilanes as Anchoring Groups for Phenylene-Thiophene Molecular Monolayer Field Effect Transistors

*Adam V. S. Parry, Kexin Lu, Daniel J. Tate, Barbara Urasinska-Wojcik, Dolores Caras-Quintero, Leszek A. Majewski, and Michael L. Turner**

Self assembled monolayer field effect transistors (SAMFETs) are reported using a phenylene-thiophene containing semiconducting mesogen attached through a trichlorosilane anchoring group. Monolayer films, covalently attached to silicon dioxide substrates, form in less than 10 h from solution, thanks to the accelerated reaction of the trichlorosilane anchor. Devices exhibit mobilities as high as 1.7×10^{-2} cm^2 V^{-1} s^{-1}, currents of up to 15 μA (on/off current ratio of 10^6) with device yields close to unity over large areas for channel lengths up to 100 μm.

1. Introduction

Self assembled monolayers (SAMs) are dense molecular layers deposited at an interface spontaneously from solution. They have become a critical technology in organic electronics for the deposition of functional nanoscale films from the bottom up. SAMs have been extensively used to modify the surface of dielectric layers and metal electrodes but have recently shown great promise as single molecular layer dielectrics or semiconductors in organic field effect transistors (OFETs).[1–16]

Self assembled monolayer field effect transistors (SAMFETs) have been demonstrated consisting of a single molecular layer of organic semiconductor, self assembled from solution.[8–14,16] The principal building blocks of these devices are molecules with a π-conjugated semiconducting core that is coupled to a surface anchoring group capable of covalently binding to a surface. These molecules create a self-limiting monolayer between source and drain contacts that functions as a two dimensional charge transport layer, comparable in thickness to the charge accumulation layer in a device. Thanks to this two dimensional transport layer SAMFETs show great potential in the field of chemical sensors where direct access to the charge transport layer by analytes will have a strong influence on the device properties.

Early attempts to fabricate SAMFETs resulted in poor performance at channel lengths >1 μm, due to high contact resistance and poor long range order of the π-conjugated cores.[14,16] The breakthrough was achieved when Smits et al. reported a SAMFET molecule consisting of a monochlorosilane anchoring group separated from a quinquethiophene core by an alkyl spacer.[12] The molecule showed long range order when deposited onto a silicon dioxide surface and field effect characteristics could be obtained over large areas for channel lengths up to 40 μm. SAMFETs have now been reported using phosphonic acid anchoring groups to covalently attach to aluminum oxide and alternative aromatic cores to create p- and n-type transistors over long channel lengths.[8–11,17,25,26]

Herein, we report a novel p-type SAMFET molecule anchored through a trichlorosilane to give working field effect transistors for devices with long channel lengths (100 μm). The use of a trichlorosilane allows an accelerated deposition of a continuous monolayer over large areas with minimal post processing. The films were characterized by atomic force microscopy (AFM), X-ray photoelectron spectroscopy (XPS) and variable angle attenuated total reflectance – Fourier transform infrared (VATR-FTIR) spectroscopy.

2. Results and Discussion

2.1. Molecular Design Considerations

The choice of the semiconducting core of the SAM molecule is crucial to the realization of high-performance SAMFETs with a dense and ordered semiconducting monolayer. It has been recognized that conjugated mesogens can be self-organized into large area monodomains without defects caused by grain boundaries by processing in the mesophase.[18,19] Conjugated mesogens based on a phenylene-bithiophene core (PTTP) are promising semiconductors employed in OFETs due to the simple synthesis and favorable liquid crystalline phase behavior.[19–21] Further, the introduction of the phenylene units lowers the HOMO level leading to improved device stability in

Dr. A. V. S. Parry, Dr. K. Lu, Dr. D. J. Tate,
Dr. B. Urasinska-Wojcik, Dr. D. Caras-Qintero,
Prof. M. L. Turner
School of Chemistry
University of Manchester
Manchester M13 9PL, UK
E-mail: michael.turner@manchester.ac.uk
Dr. L. A. Majewski
School of Electronics and Electronic Engineering
University of Manchester
Manchester M13 9PL, UK

DOI: 10.1002/adfm.201401392

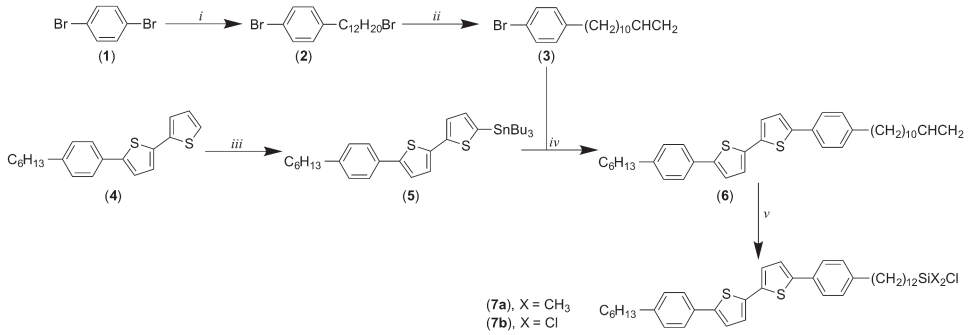

Scheme 1. Synthetic scheme for synthesis of SAMFET materials, compounds **7a** and **7b**. Reagents: *i*) 1. *n*-BuLi,/THF, 2. 1,12-dibromododecane, 71%; *ii*) *t*BuOK/THF, 95%; *iii*) 1. *n*-Buli/THF 2. Bu_3SnCl, 84%; *iv*) $Pd(PPh_3)_4$/DMF/ Δ, 85%; *v*) Karstedt's Catalyst/SiX_2ClH/toluene/Δ, 100%.

ambient, humid conditions relative to that of the analogous oligothiophenes. The sequence of liquid crystalline phases (I-SmA-G), in a PTTP mesogen, allowed melt processing of homeotropically aligned films and strong intermolecular π–π interaction between adjacent molecules.[19] Hence, PTTP was chosen as the semiconducting core for the molecular monolayer, n-hexyl (C_6) chain as the end-capping group and a flexible dodecane (C_{12}) spacer linked the semiconducting core to the trichlorosilane anchoring group.

2.2. Synthesis

Compounds **7a** and **7b** were prepared as depicted in **Scheme 1**. In brief, **1** was lithiated with *n*-BuLi, followed by workup with 1,12-dibromododecane to afford **2**, which in turn underwent dehydrohalogenation upon treatment with *t*BuOK. Compound **4** was prepared according to the procedure of Hu et al.[22] Treatment with *n*-BuLi and tributyltin chloride afforded **5**. Stille cross coupling between **3** and **5** with $Pd(PPh_3)_4$ in DMF proceeded smoothly to yield compound **6** in excellent yield. Hydrosilylation of **6** with dimethylchlorosilane or trichlorosilane afforded compounds **7a** and **7b** respectively in near quantitative conversion under optimum conditions determined by Ponomarenko et al. (33 ppm Pt, 80 eq silane, 90 °C).[23] Compound **6** exhibited a narrow smectic mesophase between 214 °C and 218 °C indicated by a typical fan texture when viewed between crossed polarizers (see Supporting Information).

2.3. Fabrication of SAMs and Devices

Highly doped (n++) silicon substrates with 300 nm of thermally grown oxide were used as the gate electrode and dielectric respectively. To enhance the anchoring of the silanes to the silicon dioxide the substrates were rinsed and sonicated in acetone, propan-2-ol and methanol followed by activation in UV-Ozone. The substrates were transferred into a nitrogen glove box and placed in a sealed vessel containing a solution of compound **7a** or **7b** in chloroform at a concentration of 0.5 mg mL^{-1} (3 mM) that had been filtered through a 0.2 μm PTFE syringe filter. The substrates were incubated in this solution for between 1 h and 7 days, transferred to a vial of clean solvent and sonicated for 30 minutes to remove physisorbed material and impurities, followed by drying under a stream of nitrogen. The substrates were annealed on a hot plate for 2 h at 120 °C to remove residual solvent. Transistors were completed by the evaporation of gold source and drain electrodes through a shadow mask to a nominal thickness of 50 nm.

The monochlorosilane (**7a**) showed a very low reactivity at a silicon dioxide surface and it was not possible to form complete monolayers from this compound, in contrast to the previously reported quinquethiophene derivative.[12] The trichlorosilane derivative (**7b**) was more reactive and working monolayer field effect transistors were fabricated in less than 10 h over large areas (4 cm^2) for long channel lengths (up to 100 μm).

2.4. Monolayer Analysis

2.4.1. Atomic Force Microscopy

The growth and morphology of the SAMs formed by deposition of **7a** and **7b** were investigated by atomic force microscopy. The monochlorosilane derivative (**7a**) exhibited a slow growth rate and incomplete monolayer formation was observed even after several days in solution. After 1 day (Figure S14, Supporting Information) the islands are small (<100 nm) and cover approximately 25% of the surface. A line scan shows that the islands are approximately 3 nm in height, which is slightly lower than the predicted height of **7a** (3.5 nm), suggesting that the molecules are tilted toward the substrate surface. The presence of larger islands, with a larger height profile (4.5 nm) suggests that these molecules stand in a more upright position. After immersion for 3 days the coverage increases to approximately 35% with the formation of some larger islands and aggregates that could not be removed by sonication. It appears that the condensation reaction between the surface and the chlorosilane is so slow that the solution reaches equilibrium with the substrate. The interaction between the conjugated semiconducting core and the polar silicon dioxide inhibits the growth of full monolayer films. Attempts to fabricate OFET devices led to insulating properties due to limited percolation paths for charge carriers between the source and drain electrodes. NMR spectroscopy of aliquots taken during the deposition process confirmed that a large portion of the solution was still in the form of free monochlorosilane (identified by the presence of the two methyl groups bonded to silicon,

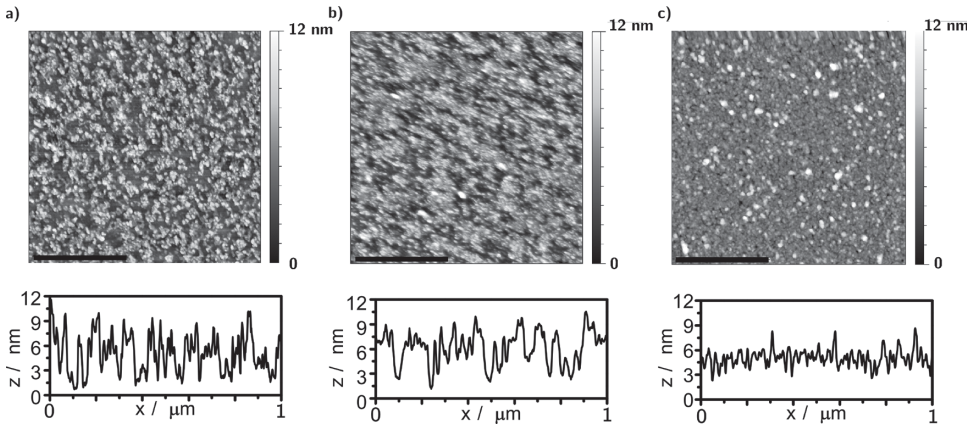

Figure 1. Atomic force microscopy topography images of compound **7b** growing on silicon dioxide substrates after a) 1, b) 3, and c) 9 h in solution, with corresponding line scans, scale bar is 400 nm.

$\delta = 0.41$ ppm) confirming that the lack of full coverage was not due to consumption of **7a** by self-condensation in solution.

The increased reactivity of the trichlorosilane derivative (**7b**) was aided by the higher solubility of **7a** over **7b**, reducing the amount of solution aggregation possible during monolayer formation. **Figure 1** shows the growth of **7b** on silicon dioxide, after 1 hour the surface coverage is already greater than 60%, after 3 hours the coverage increases to 90% and complete coverage is observed after 9 hours. As with the monochlorosilane, compound **7b** grows in the form of small islands (<100 nm) that are distributed homogeneously across the surface and ultimately lead to the formation of crystalline monolayers with little or no grain boundaries.

It has been seen that monochlorosilanes have different self assembly kinetics than the corresponding di- and tri-chloro derivatives.[27] In order to gain some insight into our system a simple, first order, Langmuir kinetics model was used to estimate the rate constants for the two systems.[28] Fitting the model to the coverage measured from the AFM images showed that the rate constant for the trichlorosilane compound (0.23 s^{-1}), is five times greater than that of the monochlorosilane derivative (0.04 s^{-1}) (see Supporting Information for details of the calculation).

Complete monolayers of **7b** have a surface roughness of ≈2 nm. Working devices were successfully fabricated from these films, even at large channel lengths (100 µm), confirming the long range order of the molecular monolayer. The choice of trichlorosilane anchoring group allows for a crosslinking of the molecules within the film, improving film stability and potentially benefitting the molecular packing and overall device performance. Previous work has shown that trichlorosilane SAMs generally lead to higher grafting densities and smaller tilt angles than mono- or di-chlorosilane derivatives,[29] In SAMFET devices the improved molecular packing of these SAMs should translate to higher device performance.

2.4.2. X-Ray Photon Electron Spectroscopy

X-ray photon electron spectroscopy was performed on both compounds **7b** (trichlorosilane) and **7a** (monochlorosilane) deposited on to silicon dioxide substrates (see Supporting Information for further details). All spectra confirm the presence of carbon and sulphur. The calculated sulphur to carbon ratio for compound **7b** is 2/38 = 0.053, the measured value from XPS of 0.051 is confirmation of surface coverage by the semiconducting molecular monolayer. Films derived from compound **7a** (monochlorosilane), which formed incomplete monolayers, showed the presence of chlorine in the XPS spectra, indicating unreacted species within the film. In contrast films deposited from the trichlorosilane derivative **7b** contained no chlorine and it can be postulated that the monolayer has completely reacted with the surface and that a significant portion of the film has crosslinked.

2.4.3. Variable Angle, Attenuated Total Reflectance – FTIR

The position of C-H stretching frequencies for the alkyl chains of a SAM observed in the IR spectrum gives information about the degree of crystallinity within a monolayer.[1,24] To investigate the degree of crystallinity of films of compound **7b**, SAMs were deposited on the native oxide of bare silicon substrates and investigated by variable angle ATR infra red spectroscopy (VATR-FTIR). Spectra were recorded at a resolution of 2 cm^{-1} and a total of 1024 scans were averaged. **Figure 2** shows the C-H stretching region of the IR spectrum. The peaks are assigned as follows, symmetric and asymmetric CH_2 absorptions ($\nu_s(CH_2)$, $\nu_a(CH_2)$) are observed at 2851.6 cm^{-1} and 2919.2 cm^{-1} respectively, the symmetric CH_3 ($\nu_s(CH_3)$) absorption appears at 2879.7 cm^{-1} and the in-plane CH_3($\nu_a(CH_3$,ip)) at 2964.7 cm^{-1}. The out-of-plane CH_3 and Fermi resonance splitting of the symmetric CH_3 were obscured by the other peaks. **Table 1** compares the peak positions of the CH stretches observed for the SAMFET (**7b**) film with those assigned for crystalline and liquid alkanes and a crystalline octadecyltrichlorosilane (OTS) monolayer film (Supporting Information Figure S20).[24] The SAMFET films are consistent with a highly crystalline molecular monolayer demonstrating the potential of this molecule for large area deposition of well-ordered monolayers.

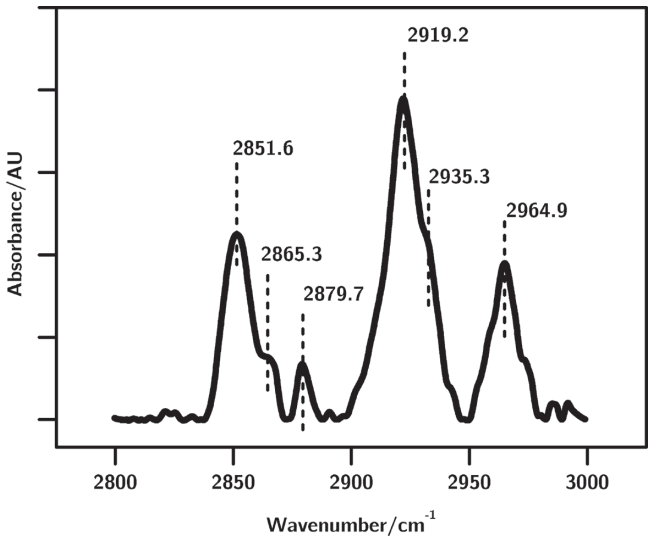

Figure 2. VATR-FTIR spectra of compound **7b** on bare silicon/native oxide substrates. Peak positions confirm the crystalline nature of the alkyl chains within the monolayer (Table 1).

Table 1. VATR-FTIR C-H stretches of the SAMFET (**7b**) referenced to liquid and crystalline peaks as described in the text.

Stretching Mode	Crystalline[a)] [cm^{-1}]	Liquid[a)] [cm^{-1}]	Spin Cast OTS[b)] [cm^{-1}]	SAMFET [cm^{-1}]
$\nu_a(CH_2)$	2918	2924	2918.3	2919.2
$\nu_s(CH_3)$	2851	2855	2850.8	2851.6
$\nu_a(CH_3,ip)$	–	–	2965.7	2964.7
$\nu_a(CH_3,op)$	2956	2957	2956.4	–
$\nu_s(CH_3)$	–	–	2878.7	2879.7
$\nu_s(CH_3,FR)$	–	–	2936.1	–

[a)]Taken from the literature;[24] [b)]See Supporting Information

2.5. Transistor Characterization

Typical transfer and output characteristics for a device with full monolayer coverage (channel length of 90 µm, channel width of 2000 µm) are presented in **Figure 3**. The saturation and linear mobility of the transistor was found to be 1.6×10^{-2} cm^2 V^{-1} s^{-1} and 1.7×10^{-2} cm^2 V^{-1} s^{-1} respectively, with an on/off current ratio of greater than 10^6 and an onset voltage close to zero. Functioning devices were observed for all channel lengths (20–100 µm) and a device yield of 100% was obtained (out of 36 devices tested), confirming the large area applicability of the fabrication procedure. Good electrical charge injection from the contacts is confirmed by the linearity in the output characteristics passing through the origin.

The dependence of the saturation and linear mobility on channel length (20–100 µm) are presented in **Figure 4** for 9 devices fabricated on the same substrate. In general the linear mobility is slightly higher than the saturation mobility but both parameters show the same dependence on the channel length. Below 50 µm the mobility reduces as a consequence of the increased contribution from contact resistance at these shorter channel lengths. For long channel lengths (>40 µm) the mobility plateaus and stays the same up to the maximum channel length of 100 µm. The consistent mobility at channel lengths greater than 40 µm is confirmation of long-range charge transport through a densely packed monolayer with minimal conduction barriers arising from grain boundaries or incomplete coverage. Similar behavior was reported by Mathijssen et al., who reported that the exponential decay of mobility with channel length seen in earlier attempts at creating SAMFETs was a result of incomplete coverage.[30]

Other extracted parameters, threshold voltage, subthreshold swing and hysteresis, remain constant for all channel lengths and are presented in **Table 2** along with the saturation and linear mobility. The averages are taken over all devices with channel lengths greater than 40 µm (total of 24 devices).

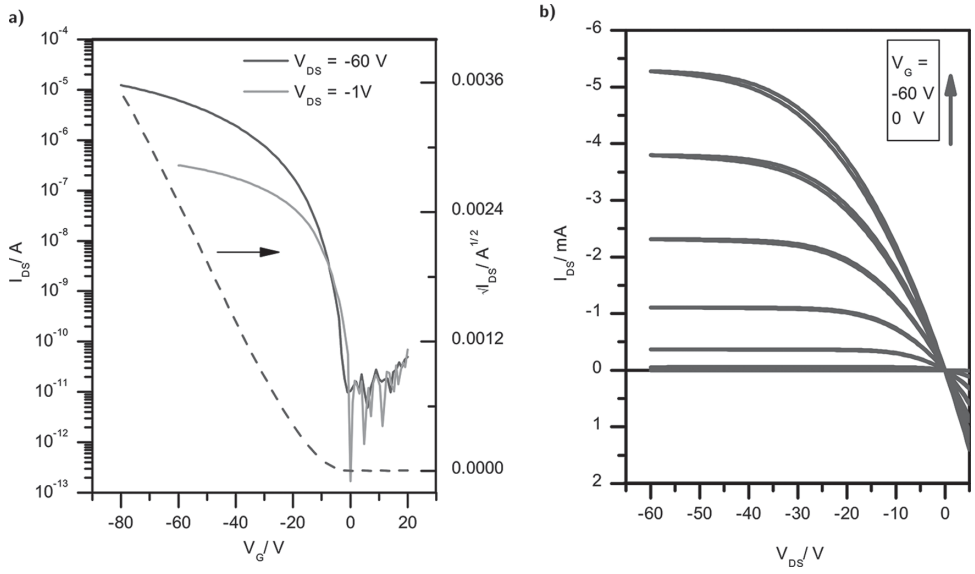

Figure 3. a) Saturation (black line) and linear (grey line) transfer characteristics, and b) output and hysteresis characteristics of transistors fabricated from compound **7b**. Channel length of 90 µm and channel width of 2000 µm.

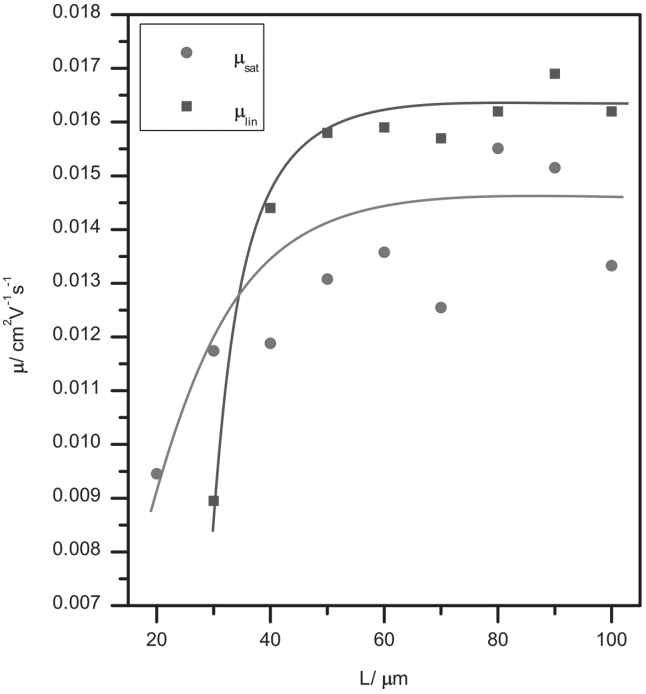

Figure 4. Mobility (μ) vs channel length (L) in the saturation (circles) and linear (squares) regime for devices fabricated on one substrate. Increase in mobility is due to a decreased contribution from contact resistance at longer channel lengths (Supporting Information).

3. Conclusion

To summarize, a novel self assembled monolayer field effect transistor (SAMFET) has been produced, demonstrating an average saturation mobility of 1.5×10^{-2} cm^2 V^{-1} s^{-1}. Large-area, high yield monolayer devices have been fabricated, in less than 10 hours on a silicon dioxide surface by utilizing a trichlorosilane anchoring group. These monolayer devices showed high mobilities, on the order of magnitude of the highest reported SAMFETs to date, confirming the promising choice of this semiconducting core. The good performance demonstrates the long-range order, high coverage and good connectivity within the SAM films. These thin films have great promise for sensing applications as the ultrathin monolayer thickness could lead to improved sensitivity to analytes in these devices over the comparable bulk devices. Furthermore, the covalently bound monolayer films offer stability against delamination in the presence of solvents.

Table 2. Parameters extracted from transfer curves. μ_{sat} is the saturation mobility, μ_{lin} is the linear mobility, V_{th} is the threshold voltage, SS is the subthreshold swing, and Hys is the hysteresis. The averages are taken over all devices with channel lengths above 40 μm. Errors correspond to the standard deviation over 4 devices.

	μ_{sat} [cm^2 V^{-1} s^{-1}]	μ_{lin} [cm^2 V^{-1} s^{-1}]	V_{th} [V]	SS [V dec^{-1}]	Hys [V]
Average	$1.39 \pm 0.1 \times 10^{-2}$	$1.61 \pm 0.1 \times 10^{-2}$	-18.2 ± 3	0.84 ± 0.3	3 ± 1
Best	1.6×10^{-2}	1.7×10^{-2}	−20	0.70	2.6

4. Experimental Section

Further information on film characterization, atomic force microscopy, X-ray photoelectron spectroscopy, IR and electrical measurements can be found in the Supporting Information.

Monolayer Preparation: Solutions were prepared in an inert atmosphere to the desired concentration with the chosen solvent. The solutions were then heated to approximately 40 °C to facilitate the solvation of all of the material. They were then left to stand until reaching room temperature where they were then filtered through a 0.2 μm syringe filter into a sealed container with the freshly cleaned substrates. After the desired immersion time the substrates were transferred to sealed jars containing fresh solvent, removed from the inert atmosphere and sonicated for approximately 30 min. The clean substrates were finally dried on a hotplate at 120 °C for 2 h.

Atomic Force Microscopy (AFM): AFM images were recorded on a Bruker Multimode 8 in Peak Force tapping mode at a resolution of 512 × 512 pixels. Cantilevers had a spring constant of approximately 0.350 Nm^{-1} with a resonant frequency of approximately 50–80 kHz. A modulation frequency of 2 kHz was used.

X-Ray Photoelectron Spectroscopy (XPS): XPS measurements were performed using a Kratos Axis Nova with a monochromated aluminum Kα X-ray source (1486.69 eV). Detailed spectra of individual peaks were taken at energy of 20 eV with a step size of 0.1 eV with a power of 225 W. The spectra were analyzed using CasaXPS.

Variable Angle Attenuated Total Reflectance-Fourier Transform Infrared (VATR-FTIR) Spectroscopy: Monolayers were prepared on bare silicon substrates as this enhances the attenuation of the IR radiation. A Bruker Vertex 70 equipped with a Harrick Seagull ATR accessory and a germanium crystal is used in conjunction with a MCT detector. The sample is brought into contact with the crystal by applying a torque of 7.4 in.lbs to the sample mount. The angle of incidence of the source was 65 °. Both the background and the sample spectra were recorded at a resolution of 2 cm^{-1} for a total of 1024 scans.

Transistor Characterization: Transistors were tested in a top contact, bottom gate geometry. Thermally grown silicon dioxide (IDB Technologies) was used as the gate dielectric with a thickness of approximately 300 nm and a capacitance of 11.4 nFcm^{-1}. Transfer characteristics were recorded in the saturation and linear regimes with drain voltages of −60 V and −1 V respectively. Parameter extraction was performed using the standard field effect transistor equations:

$$I_{DS} = \frac{W}{L}\mu_{lin}C_i(V_G - V_{th})V_{DS}, V_{DS} < V_G - V_{th}, \text{linear regime}$$

$$I_{DS} = \frac{W}{2L}\mu_{sat}C_i(V_G - V_{th})^2, V_{DS} > V_G - V_{th}, \text{saturation regime}$$

An Agilent B1500a equipped with 3 SMUs was used in conjunction with a probe station. All transistors were tested in air at ambient temperature and pressure.

Synthesis—General Considerations: Unless stated otherwise, all reagents and solvents were obtained from commercial suppliers and used without further purification. Anhydrous THF was pre-dried over sodium wire prior to continuous distillation over sodium-benzophenone under an atmosphere of argon. Other anhydrous solvents were used as supplied (water content < 0.05%). ^{1}H and ^{13}C{^{1}H} NMR spectra were recorded on a Bruker 400 MHz or 500 MHz spectrometer. The progress of reactions was monitored by TLC on pre-coated silica or alumina plates visualized by ultraviolet light or staining with vanillin or potassium permanganate in the absence of a chromophore. Column chromatography employed Merck Kieselgel (60 Å) F_{254} (230–400 mesh) silica or Aldrich neutral alumina and HPLC grade solvents. Distillation was carried out using standard Kugelrohr equipment with an oil diffusion pump. Purification by recrystallization refers to the process of repeated recrystallization to a constant melting point. Melting points were recorded on a Linkam LTSE350 heating stage, quoted in degrees Celsius (°C) and are uncorrected.

1-Bromo-4-(12-bromododecyl)benzene (2): n-Butyllithium (2.5 M, 16.95 mL, 42.39 mmol) was added dropwise to a flame dried flask charged with 1,4-dibromobenzene (10.0 g, 42.39 mmol) dissolved in anhydrous THF (150 mL) cooled to −78 °C under and argon atmosphere. Upon completion of the addition, stirring at −78 °C was continued for 30 min, whereby a fine white precipitate formed. The precipitate was transferred via cannula rapidly to a second flame dried flask charged with 1,12-dibromododecane (34.77 g, 105.97 mmol) dissolved in anhydrous THF (250 mL) cooled to −78 °C under an argon atmosphere. Upon completion of the transfer, the mixture was stirred at −78 °C for 60 min and allowed to warm to room temperature and stirred overnight. The reaction was quenched with sat. NH_4Cl (20 mL), diluted with Et_2O (500 mL), washed successively with water (2 × 100 mL), brine (2 × 100 mL), dried ($MgSO_4$) and concentrated in vacuo to afford a crude oil, which was purified by short path distillation. Excess 1,12-dibromododecane was first isolated (bp 110 °C, 5×10^{-6} mbar) followed by the title compound (12.20 g, 71%) (bp 180 °C, 5×10^{-6} mbar), which crystallised on standing, mp 37 °C. ^{1}H NMR (400 MHz, $CDCl_3$, δ): 7.39 (d, J = 8.40 Hz, 2H), 7.07 (d, J = 8.40 Hz, 2H), 3.43, (t, J = 6.88 Hz, 2H), 2.57 (t, J = 7.56 Hz, 2H), 1.91 – 1.83 (m, 2H), 1.61 – 1.54 (m, 2H), 1.45 – 1.35 (m, 2H), 1.31 – 1.25 (m 14H); ^{13}C{^{1}H} NMR (100 MHz, $CDCl_3$, δ): 141.8, 131.2, 130.2, 119.2, 35.4, 34.1, 32.8, 31.3, 29.6, 29.52, 29.50, 29.44, 29.41, 29.2, 28.8, 28.2; IR (ATR): $\bar{\nu}_{max}$ (cm^{-1}) 3077, 2918, 2849, 1458, 1203, 1076, 997; HRMS (EI+) m/z [M]$^+$ calcd for $C_{18}H_{28}Br_2$, 402.0552; found 402.0557. Anal. calcd for $C_{18}H_{28}Br_2$: C 53.48, H 6.98, Br 39.53; found: C 53.68, H 6.99, Br 39.87.

1-Bromo-4-(dodec-11-en-1-yl)benzene (3): Potassium *tert*-butoxide (2.78 g, 24.74 mmol) and **2** (5.0 g, 12.37 mmol), dissolved in anhydrous THF (100 mL), were stirred at reflux under an atmosphere of argon for 3 hours. The reaction was allowed to cool to room temperature, filtered to remove inorganic salts and the filtrand was washed with hexane (2 × 100 mL). The combined organic filtrate were concentrated in vacuo. The residue was dissolved in hexane (250 mL), washed successively with water (2 × 100 mL), brine (2 × 100 mL), dried ($MgSO_4$) and concentrated in vacuo. The residue was purified by column chromatography, eluting with hexane (Rf ≈ 0.60) to afford the title compound (3.79 g, 95%) as a colorless oil. ^{1}H NMR (400 MHz, $CDCl_3$, δ): 7.40 (d, J = 8.32 Hz, 2H), 7.06 (d, J = 8.32 Hz, 2H), 5.87 – 5.80 (m, 1H), 5.03 – 4.94 (m, 2H), 2.57 (t, J = 7.56 Hz, 2H), 2.08 – 2.03 (m, 2H), 1.62 – 1.57 (m, 2H), 1.41 – 1.28 (m, 14H); ^{13}C{^{1}H} NMR (100 MHz, $CDCl_3$, δ): 141.9, 139.3, 131.2, 130.2, 119.2, 114.1, 35.4, 33.8, 31.3, 29.6, 29.5, 29.47, 29.44, 29.2, 29.1, 28.9; IR (ATR): $\bar{\nu}_{max}$ (cm^{-1}) 3077, 2918, 2849, 1642, 1498, 1458, 1076; HRMS (EI+) m/z [M]$^+$ calcd for $C_{18}H_{27}Br$, 322.1291; found 322.1287. Anal. calcd for $C_{18}H_{27}Br$: C 66.87, H 8.42, Br 24.71; found: C 67.02, H 8.32, Br 24.73.

5-(Tri-n-butylstannyl)-5-(4-n-hexylphenyl)-2,2'-bithiophene (5) : To a flame dried flask under argon, was charged **3** (10.0 g, 30.62 mmol) and anhydrous THF (250 mL). The reaction was cooled to −30 °C and butyllithium (12.82 mL, 32.16 mmol, 2.5 M in hexanes) was added drop wise over 30 min. After stirring for an additional hour at −30 °C, tributyltin chloride (9.14 mL, 33.69 mmol) was added drop wise over 20 min. The reaction was allowed to equilibrate to room temperature overnight and potassium fluoride (1.4 g, 24.10 mmol) was added in a single portion. After stirring for 1 h the reaction was filtered to remove the inorganic salts. The filtrate was diluted with hexane (300 mL), washed successively with sat. $NaHCO_3$ (3 × 100 mL), water (3 × 100 mL), brine (2 × 100 mL), dried (MgSO4) and concentrated in vacuo. The crude was purified over Brockmann grade II alumina eluting with hexane to afford the title compound as a yellow/green oil (15.86 g, 84%). ^{1}H NMR (400 MHz, $CDCl_3$, δ): 7.52 (d, J = 8.20 Hz, 2H), 7.32 (d, J = 3.36 Hz, 1H), 7.20 (d, J = 8.20 Hz, 2H), 7.20 (d, J = 3.76 Hz, 1H) 7.15 (d, J = 3.76 Hz, 1H), 7.09 (d, J = 3.36 Hz, 1H), 2.63 (t, J = 7.80 Hz, 2H), 1.68 – 1.53 (m, 8H), 1.41 – 1.28 (m, 12H), 1.16 – 1.12 (m, 6H), 0.93 (t, J = 7.28 Hz, 12H); ^{13}C{^{1}H} NMR (100 MHz, $CDCl_3$, δ): 142.9, 142.8, 136.6, 136.5, 136.1, 131.6, 128.9, 125.5, 124.7, 124.3, 123.2, 35.7, 31.7, 31.4, 29.0, 28.96, 27.3, 22.6, 14.1, 13.7, 10.9.

5-(4-Dodec-11-en-1-yl)phenyl)-5'-(4-hexylphenyl)-2,2'-bithiophene (6): Tetrakis(triphenylphosphine)palladium(0) (162.5 mg, 0.14 mmol, 2 mol%) was added under a fast stream of argon to a flame dried flask charged with **5** (4.07 g, 7.03 mmol) and **3** (2.5 g, 7.73 mmol) dissolved in degassed anhydrous DMF (80 mL). The reaction mixture was degassed for a further hour and brought to 80 °C for 16 h. Upon completion of the reaction, it was allowed to cool to room temperature and poured on to methanol (250 mL). The resultant precipitate was filtered and the filtrand was dry loaded on to silica and filtered through a silica/Celite plug eluting with DCM. The filtrate was concentrated in vacuo to afford the title compound (3.41 g, 85%), which was recrystallized from toluene to yield a bright yellow precipitate. mp 218 °C; ^{1}H NMR (400 MHz, $CDCl_3$, δ): 7.54 (d, J = 8.12 Hz, 4H), 7.21 – 7.16 (m, 6H), 7.16 (d, J = 3.80 Hz, 2H), 5.89 – 5.80 (m, 1H), 5.03 – 4.93 (m, 2H), 2.64 (t, J = 7.68 Hz, 4H), 2.09 – 2.03 (m, 2H), 1.68 – 1.61 (m, 4H), 1.39 – 1.29 (m, 24H), 0.92 (t, J = 6.76 Hz, 3H); ^{13}C{^{1}H} NMR (100 MHz, $CDCl_3$, δ): 143.3, 142.6, 139.3, 136.3, 131.5, 129.0, 125.5, 124.3, 123.3, 114.1, 35.7, 33.8, 31.7, 31.40, 31.37, 29.59, 29.57, 29.5, 29.3, 29.2, 28.98, 28.95, 22.6, 14.1; IR (ATR): $\bar{\nu}_{max}$ (cm^{-1}) 3077, 2918, 2849, 1642, 1498, 1458, 1314, 1124, 1076, 997; HRMS (EI+) m/z [M]$^+$ calcd for $C_{38}H_{48}S_2$, 568.3192; found 568.3195. Anal. calcd for $C_{38}H_{48}S_2$: C 80.22, H 8.50, S 11.27; found: C 80.10, H 8.84, S 11.26.

Chloro(12-(4-(5-(5-(4-hexylphenyl)thiophen-2-yl)thiophen-2-yl)phenyl) dodecyl)dimethylsilane (7a): Under vacuum, assembled, flame dried glassware was transferred to a nitrogen glove box. The glassware was charged with **6** (500 mg, 0.939 mmol), anhydrous toluene (55.5 mL), Karstedt's catalyst (92 µL, 33 ppm Pt) and chlorodimethylsilane (8.34 mL, 75.3 mmol, 80 eq). The glassware was sealed and brought to 90 °C overnight. The reaction was allowed to cool and evaporated to dryness with stirring under vacuum. The nitrogen purged glassware was transferred to a high vacuum turbo pump and dried thoroughly at room temperature (7×10^{-8} mbar) for 2 h to afford the title compound as a bright yellow powder (quantitative conversion). The evacuated flask was once again passed into a nitrogen glovebox for storage and handling. ^{1}H NMR (500 MHz, $CDCl_3$, δ): 7.53 (d, J = 8.15 Hz, 4H), 7.21 – 7.17 (m, 6H), 7.15 (d, J = 3.75 Hz, 2H), 2.63 (t, J = 7.75 Hz, 4H), 1.66 – 1.58 (m, 4H), 1.37 – 1.19 (m, 22H), 0.90 (t, J = 6.85 Hz, 3H), 0.41 (s, 6H).

Trichloro(12-(4-(5'-(4-hexylphenyl)-[2,2'-bithiophen]-5-yl)phenyl) dodecyl)silane (7b): Under vacuum, assembled, flame dried glassware was transferred to a nitrogen glove box. The glassware was charged with **6** (500 mg, 0.939 mmol), anhydrous toluene (55.5 mL), Karstedt's catalyst (92 µL, 33 ppm Pt) and trichlorosilane (7.58 mL, 75.3 mmol, 80 eq). The glassware was sealed and brought to 90 °C overnight. The reaction was allowed to cool and evaporated to dryness with stirring under vacuum. The nitrogen purged glassware was transferred to high vacuum turbo pump and dried thoroughly at room temperature (7×10^{-8} mbar) for 2 hours to afford the title compound as a bright yellow powder. The evacuated flask was once again passed into a nitrogen glovebox for storage and handling. ^{1}H NMR (500 MHz, $CDCl_3$, δ): 7.52 (d, J = 8.20 Hz, 4H), 7.21 – 7.17 (m, 6H), 7.15 (d, J = 3.75 Hz, 2H), 2.65 (t, J = 7.70 Hz, 4H), 1.66 – 1.55 (m, 4H), 1.42 – 1.26 (m, 22H), 0.90 (t, J = 6.85 Hz).

Supporting Information

Supporting Information is available from the Wiley Online Library or from the author.

Acknowledgements

The authors wish to thank the EPSRC for financial support for a NowNano PhD studentship for AVSP and for grant EP/C523857/1. They also wish to thank Dr. S. A. Ponomarenko and Prof. D. M. de Leeuw for their helpful discussions concerning the hydrosilylation of alkenes. X-ray photoelectron spectra were obtained at the National EPSRC XPS Service (NEXUS) at Newcastle University, an EPSRC Mid-Range Facility.

Received: April 29, 2014
Revised: June 16, 2014
Published online: August 26, 2014

[1] Y. Ito, A. A. Virkar, S. Mannsfeld, J. H. Oh, M. Toney, J. Locklin, Z. Bao, *J. Am. Chem. Soc.* **2009**, *131*, 9396–9404.
[2] A. Virkar, S. Mannsfeld, J. H. Oh, M. F. Toney, Y. H. Tan, G.-Y. Liu, J. C. Scott, R. Miller, Z. Bao, *Adv. Funct. Mater.* **2009**, *19*, 1962–1970.
[3] H. Yang, T. J. Shin, M.-M. Ling, K. Cho, C. Y. Ryu, Z. Bao, *J. Am. Chem. Soc.* **2005**, *127*, 11542–11543.
[4] M. Halik, H. Klauk, U. Zschieschang, G. Schmid, C. Dehm, M. Schütz, S. Maisch, F. Effenberger, M. Brunnbauer, F. Stellacci, *Nature* **2004**, *431*, 963–966.
[5] H. Ma, O. Acton, G. Ting, J. W. Ka, H.-L. Yip, N. Tucker, R. Schofield, A. K.-Y. Jen, *Appl. Phys. Lett.* **2008**, *92*, 113303.
[6] H. Klauk, U. Zschieschang, J. Pflaum, M. Halik, *Nature* **2007**, *445*, 745–748.
[7] T. Sekitani, U. Zschieschang, H. Klauk, T. Someya, *Nat. Mater.* **2010**, *9*, 1015–1022.
[8] T. Schmaltz, A. Y. Amin, A. Khassanov, T. Meyer-Friedrichsen, H.-G. Steinrück, A. Magerl, J. J. Segura, K. Voitchovsky, F. Stellacci, M. Halik, *Adv. Mater.* **2013**, *25*, 4511–4514.
[9] A. Ringk, X. Li, F. Gholamrezaie, E. C. P. Smits, A. Neuhold, A. Moser, C. Van der Marel, G. H. Gelinck, R. Resel, D. M. de Leeuw, P. Strohriegl, *Adv. Funct. Mater.* **2013**, *23*, 2016–2023.
[10] N. Cernetic, O. Acton, T. Weidner, D. O. Hutchins, J. E. Baio, H. Ma, A. K.-Y. Jen, G. Ting, D. G. Castner, *Org. Electron.* **2012**, *13*, 3226–3233.
[11] M. Novak, A. Ebel, T. Meyer-Friedrichsen, A. Jedaa, B. F. Vieweg, G. Yang, K. Voitchovsky, F. Stellacci, E. Spiecker, A. Hirsch, M. Halik, *Nano Lett.* **2011**, *11*, 156–159.
[12] E. C. P. Smits, S. G. J. Mathijssen, P. A. van Hal, S. Setayesh, T. C. T. Geuns, K. A. H. A. Mutsaers, E. Cantatore, H. J. Wondergem, O. Werzer, R. Resel, M. Kemerink, S. Kirchmeyer, A. M. Muzafarov, S. A. Ponomarenko, B. de Boer, P. W. M. Blom, D. M. de Leeuw, *Nature* **2008**, *455*, 956–959.
[13] M. Mottaghi, P. Lang, F. Rodriguez, A. Rumyantseva, A. Yassar, G. Horowitz, S. Lenfant, D. Tondelier, D. Vuillaume, *Adv. Funct. Mater.* **2007**, *17*, 597–604.
[14] X. Guo, M. Myers, S. Xiao, M. Lefenfeld, R. Steiner, G. S. Tulevski, J. Tang, J. Baumert, F. Leibfarth, J. T. Yardley, M. L. Steigerwald, P. Kim, C. Nuckolls, *Proc. Natl. Acad. Sci. U.S.A.* **2006**, *103*, 11452–11456.
[15] Y. Ofir, A. Zelichenok, S. Yitzchaik, *J. Mater. Chem.* **2006**, *16*, 2142–2149.
[16] G. S. Tulevski, Q. Miao, M. Fukuto, R. Abram, B. Ocko, R. Pindak, M. L. Steigerwald, C. R. Kagan, C. Nuckolls, *J. Am. Chem. Soc.* **2004**, *126*, 15048–15050.
[17] A. S. Sizov, E. V. Agina, F. Gholamrezaie, V. V. Bruevich, O. V. Borshchev, D. Y. Paraschuk, D. M. de Leeuw, S. a. Ponomarenko, *Appl. Phys. Lett.* **2013**, *103*, 043310.
[18] A. J. J. M. van Breemen, P. T. Herwig, C. H. T. Chlon, J. Sweelssen, H. F. M. Schoo, S. Setayesh, W. M. Hardeman, C. a Martin, D. M. de Leeuw, J. J. P. Valeton, C. W. M. Bastiaansen, D. J. Broer, A. R. Popa-Merticaru, S. C. J. Meskers, *J. Am. Chem. Soc.* **2006**, *128*, 2336–45.
[19] J. C. Maunoury, J. R. Howse, M. L. Turner, *Adv. Mater.* **2007**, *19*, 805–809.
[20] J. Huang, J. Sun, H. E. Katz, *Adv. Mater.* **2008**, *20*, 2567–2572.
[21] M. Mushrush, A. Facchetti, M. Lefenfeld, H. E. Katz, T. J. Marks, *J. Am. Chem. Soc.* **2003**, *125*, 9414–9423.
[22] Z. Hu, B. Fu, A. Aiyar, E. Reichmanis, *J. Polym. Sci. Part A Polym. Chem.* **2012**, *50*, 199–206.
[23] S. A. Ponomarenko, O. V. Borshchev, T. Meyer-Friedrichsen, A. P. Pleshkova, S. Setayesh, E. C. P. Smits, S. G. J. Mathijssen, D. M. de Leeuw, S. Kirchmeyer, A. M. Muzafarov, *Organometallics* **2010**, *29*, 4213–4226.
[24] M. D. Porter, T. B. Bright, D. L. Allara, C. E. D. Chidsey, *J. Am. Chem. Soc.* **1987**, *109*, 3559–3568.
[25] K. H. Lam, T. R. B. Foong, J. Zhang, A. C. Grimsdale, Y. M. Lam, *Org. Electron.* **2014**, *15*, 1592–1597.
[26] A. S. Sizov, E. V. Agina, F. Gholamrezaie, V. V. Bruevich, O. V. Borshchev, D. Y. Paraschuk, D. M. de Leeuw, S. a. Ponomarenko, *Appl. Phys. Lett.* **2013**, *103*, 043310.
[27] M. Hair, W. Hertl, *J. Phys. Chem.* **1969**, *2254*, 2372–2378.
[28] D. K. Schwartz, *Annu. Rev. Phys. Chem.* **2001**, *52*, 107–137.
[29] J. Genzer, K. Efimenko, D. A. Fischer, *Langmuir* **2002**, *18*, 9307–9311.
[30] S. G. J. Mathijssen, E. C. P. Smits, P. a van Hal, H. J. Wondergem, S. a Ponomarenko, A. Moser, R. Resel, P. a Bobbert, M. Kemerink, R. a. J. Janssen, D. M. de Leeuw, *Nat. Nanotechnol.* **2009**, *4*, 674–80.